CrystEngComm

Accepted Manuscript

ROYAL SOCIETY OF CHEMISTRY

www.rsc.org/crystengcomm

Tungsten Oxide Nanostructures Based on Laser Ablation in Water and Hydrothermal Route

Hongwen Zhang, Yue Li [*], Guotao Duan, Guangqiang Liu and Weiping Cai[*]

Key Lab of Materials Physics, Anhui Key Lab of Nanomaterials and Nanotechnology,

Institute of Solid State Physics, Chinese Academy of Sciences, Hefei 230031, P.R.

China.

Graphical Table of Contents

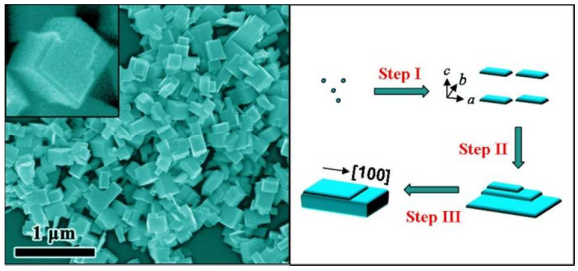

Well-dispersed and surface-stepped tungsten oxide nanostructures can be obtained via stacking of nanosized rectangular cuboids during hydrothermal treatment of LAL obtained precursors.

[*] To whom all correspondence should be addressed
E-mail: yueli@issp.ac.cn, wpcai@issp.ac.cn

ABSTRACT: A facile and chemically clean method is presented to fabricate the nanostructured tungsten oxide (WO_3), based on laser ablation of tungsten flake in water and subsequent hydrothermal route. The typically nanostructured WO_3 objects were well-dispersed and brick-like in shape. The bricks are of the average dimensions of *ca.* 200 nm in length, 150 nm in width and 130 nm in thickness, with stepped structures on their planar surfaces. Further experiments have revealed that the reaction temperature, pH value and composition of the precursor in subsequent hydrothermal treatment are crucial to formation of the brick-like WO_3 nanostructures. Correspondingly, a rectangular cuboidal stacking growth model is proposed to describe the formation of such nanobricks. The nanobricks could be the good building blocks of complex micro/nanostructures and devices. Also, the combination of laser ablation in liquid with hydrothermal treatment could provide an effective synthetic approach for morphologically tunable WO_3 nanomaterials, which have potential applications in gas sensing, electrochromic devices and photocatalysis.

Introduction

As an important wide band gap semiconductor, tungsten oxide (WO_3) has been extensively studied due to its intriguing physical and chemical properties.[1-3] Recently, the nanostructured WO_3 has attracted much attention because of its potential applications in the fields, such as electrochromic devices[4-6], gas sensors[7-10] and photocatalysts[11, 12]. Nowadays, the nanostructured WO_3 including nanowires[3, 13, 14], nanoplates[15, 16] and hierarchical micro/nanostructures[17, 18], have been successfully synthesized by some physical techniques and chemical routes. Among those approaches, hydrothermal methods have shown obvious advantages and been widely applied for fabrication of WO_3 nanostructures because of its rich modulating experimental parameters, such as chemical composition of precursors, heating temperature, pressure of reaction environment and heating durations, etc[18-20]. Besides, the cheap equipment and simple operation further facilitate fabrication of nanomaterials. Researchers have prepared various kinds of WO_3 nanostructures with varying dimensions, architectures, and morphologies. For instance, taking tungsten hexachloride (WCl_6) as raw material, Choi et.al[21] prepared WO_3 nanomaterials with modulated morphologies (from nanoparticles, nanowires to nanobelts, etc.) via hydrothermal treatment with different solvents. Therese et.al[22] obtained WO_3 nanowires with high aspect ratio by hydrothermal route using ammonium tungstate hydrate as raw material and citric acid as structure directing agent. Commonly, in addition to the low dimensional structures (nanowires, nanobelts[23, 24], nanoparticles), 3D hierarchical micro/nanoarchitectures were usually obtained through hydrothermal

approaches by simply altering types of precursors or adding capping agents. For hydrothermal preparations of WO_3 nanomaterials, it has been reported that surfactants, metal salts and organic solvents are effective capping or structure directing agents under suitable pH conditions[18, 25-28]. However, the effects of the specific additives on morphologies and the intrinsic formation mechanisms have been unclear and rarely reported. One of the most important reasons is that the utilized raw materials for precursor preparation have already contained some additives. For example, the most commonly used pristine materials are tungstate [Na_2WO_4, $(NH_4)_2WO_4$ etc] and the unavoidably adulterated cations in the precursors could also act as capping agents. Therefore, facile, green and inexpensive approaches to prepare the pure precursors for subsequent hydrothermal treatments are in urgent demands.

Pulsed laser ablation in liquid (LAL) medium is of particular interest and has been used as an effective method to fabricate the regular nanoparticles[29], metastable nanostructures[30], and even fullerene-like nanomaterials[31], due to the local and instantaneous extreme environment (ultra-high temperature and ultra-high pressure) in the liquid, induced by interaction between the pulsed laser and solid targets[32, 33]. In addition, the chemical pureness can be ensured through the selected solid targets and liquids.

Herein, we present a simple and chemically controlled method to prepare nanostructured WO_3 via the LAL method and subsequent hydrothermal treatment. In this method, colloidal solutions were firstly obtained by laser ablation of a pure tungsten target immersed in deionized water and then acidified to pH = 1.0.

Subsequently the acidified colloidal solution was hydrothermally treated. The obtained nanostructured WO_3 objects were well-dispersed and rectangular brick-like in shape. The bricks are of the average dimensions of *ca.* 200 nm in length, 150 nm in width and 130 nm in thickness, with stepped structures on their planar surfaces. Further experiments have revealed that the reaction temperature, pH value and composition of the precursor in subsequent hydrothermal treatment are crucial to formation of the brick-like WO_3 nanostructures. Such nanobricks could be the good building blocks of complex micro/nanostructures and devices. Also, the combination of laser ablation in liquid with hydrothermal treatment could provide an effective way to fabricate the morphologically tunable WO_3 nanomaterials, which have potential applications in building WO_3-based functional devices, such as electrochromic electrodes, chemical sensors and so on. The details are reported in this article.

Experimental Section

1. Laser ablation in water

The precursor (or colloidal) solutions for hydrothermal treatment were first prepared by LAL at room temperature (~25^{o}C), as previously described in details[16]. Briefly, a tungsten flake (>99.9%, 45 mm×10 mm×1 mm) was polished with emery paper and ultrasonically rinsed with deionized water and ethanol for 1 hour, respectively. The cleaned tungsten target was then immersed into a vessel filled with 30 ml of deionized water and fixed vertically. A focused Nd:YAG laser, operated at 10 Hz with a wavelength of 1064 nm and pulse duration of 10 ns, vertically irradiated on the surface of tungsten target surrounded by the deionized water. The diameter of

laser beam focused on the target was ca. 2 mm. The tungsten target was irradiated with the power 80 mJ/pulse for 120 min. The ablation medium was continuously stirred by a magnetic rotor during irradiation process. After ablation, the tungsten-contained precursor solution was obtained. The tungsten content in the solution can be estimated to be about 10mM by the mass loss of the tungsten flake.

2. Hydrothermal treatment

The as-prepared 30 ml of 10 mM tungsten-contained precursor solution was acidified to a pH value with 1.0 by slowly dropping sulfuric acid under continuous stirring. The precursor solution was subsequently transferred to a 90 ml of Teflon-lined stainless steel autoclave. The autoclave was then heated at 200 ^{o}C for 10 h before cooling to room temperature naturally. The final products were obtained by centrifugation, rinsing with deionized water and ethanol for several times, and drying at 50 ^{o}C in air.

3. Characterization

The as-obtained products were redispersed into ethanol. The corresponding film samples were prepared on glass substrates by spin-coating method for phase analysis and morphology observations. The phase structure of the products was measured using an X-ray diffractometer (XRD, the Philips X'Pert) with copper Kα radiation (0.15406 nm) at room temperature. The morphologies were observed on a field emission scanning electron microscope (FE-SEM, FEI Sirion 200). The microstructure was examined on a transmission electron microscope (TEM,

JEM-200CX). The composition was analyzed by energy-dispersive x-ray spectroscopy (EDX).

Results and Discussion

1. Colloidal precursor

After laser ablation for two hours, the as-obtained precursor solution showed yellow brown color with pH value of *ca.* 3.0. Also, Tyndall effect was observed in the solution using a laser pointer, which illustrates that the precursor is colloidal solution. Figure 1a shows an optical absorbance spectrum of the freshly obtained colloidal solution. There exists a peak around *ca.* 320 nm, which should correspond to the W-O isopolyanions.[16] The TEM observation has revealed that the colloidal precursor contains ultra-fine nanoparticles (Figure 1b). The magnified image clearly illustrates the ultra-fine nanoparticles with about 1 nm in size, as marked in the inset of Figure 1b. The selected area electronic diffraction (SAED) shows that the products are amorphous in structure. In addition, EDX measurement indicates that there only exist W and O elements in the sample, as shown in Figure 1c, in which the Cu and C signals were from the substrate. So, the colloidal solution should consists of W-O isopolyanions and amorphous ultra-fine nanoparticles.

Formation of the colloidal precursor is easily understood, as previously reported[16, 32, 33]. Briefly: (1) the tungsten plasma with high-temperature and high-pressure was produced immediately at the solid-liquid interface when pulsed laser irradiated the metal target; (2) subsequent ultrasonic and adiabatic expansion of the tungsten plasma led to quick cooling of the tungsten plume region and hence formation of tungsten

clusters; (3) the chemically active tungsten clusters react with the water molecules, producing complex isopolytungstic acid (W_xO_m•nH_2O); (4) the isopolyanions of tungsten oxide ($[W_xO_{(m+n)}]^{2n-}$) were formed via hydrolyzation of isopolytungstic acid[34]; (5) the isopolyanions further aggregated and polymerized in ill-defined degrees, resulting in the main suspension of the precursor solution ($[W_{xy}O_{(m+n)y}]^{(2ny)-}$ and W_xO_m•nH_2O). These processes can also be described by the following reactions[35].

$$W_{(bulk)} + h\upsilon \rightarrow W_{(plasma)} \quad (1)$$

$$W_{(plasma)} \rightarrow W_{(cluster)} \quad (2)$$

$$xW_{(cluster)} + (m+n)H_2O \rightarrow W_xO_m \cdot nH_2O + mH_2 \uparrow \quad (3)$$

$$W_xO_m \cdot nH_2O \rightarrow 2nH^+ + [W_xO_{(m+n)}]^{2n-} \quad (4)$$

$$y[W_xO_{(m+n)}]^{2n-} \rightarrow [W_{xy}O_{(m+n)y}]^{(2ny)-} \quad (5)$$

2. Structure and morphology

The above as-prepared colloidal solution was acidified to pH = 1.0 and subsequently hydrothermally treated. We could thus obtain the final products. Figure 2 shows the XRD pattern of the film obtained by spin-coating the products on a glass substrate. All peaks can be indexed to the monoclinic WO_3 phase with the lattice parameters of a = 0.7297 nm, b = 0.7539 nm, c = 0.7688 nm and a space group of P21/n (JCPDS No. 43-1035). In addition, the (002) reflection is significantly enhanced, indicating a preferential orientation of (002) crystal plane for the WO_3 film obtained by spin-coating.

FE-SEM observation clearly indicates that the obtained WO_3 powders consist of well-dispersed particles with dimensions of several hundred nanometers, as typically

shown in Figure 3(a, b). The particles are rectangular brick-like in shape. The nanobricks are of the average dimensions of *ca.* 200 nm in length, 150 nm in width and 120 nm in thickness. A close observation has revealed that there exist steps on some nanobricks' surfaces, as clearly demonstrated in the inset of Figure 3b.

Figure 3c gives the TEM image of some WO_3 nanobricks, which clearly exhibits the nanobricks with stepped surfaces and each step is less than 10 nm in thickness. The SAED pattern (shown in the inset of top left in Figure 3c) was acquired from an incident direction of electronic beam perpendicular to the planar surface of an isolated nanobrick as marked by an arrow in Figure 3c. It indicates single crystal diffraction pattern. The pattern can be indexed to the monoclinic WO_3 along the [010] zone axis, and the three main diffraction spots correspond to the planes of (202), ($\bar{2}02$) and (400), respectively**.** Also, the bottom right inset in Figure 3c typically shows one isolated nanobrick, and the obvious difference in contrast illustrates that the nanobrick owns three types of thicknesses (labeled with Arabic numbers of 1, 2 and 3), which further indicates the stepped structure. Based on the SAED pattern and the crystallographic character of monoclinic WO_3, directions of the three adjacent edges for the nanobrick can be indexed to [001], [010] and [100], respectively (see the bottom right inset in Figure 3c). Representatively, Figure 3d shows a typical high resolution TEM image of a partial nanobrick, and illustrates clear lattice fringes. The interplanar spacings of 0.264 and 0.268 nm can be assigned to the (202) and (220) crystal planes of monoclinic WO_3 phase, respectively. The angle between the [202] and [220] directions can be measured to be 58.2^o (see Figure 3d) which is in good

agreement with the corresponding crystallographic data (58.34°).

Based on the above analysis, we conclude that the finally obtained products, by hydrothermal treatment (200°C, 10 h) of the acidified LAL-induced colloidal solution with pH of 1.0, are well crystallized monoclinic WO_3 nanobricks with surface stepped structures.

3. Influence factors

Further experiments have revealed that formation of the WO_3 nanobricks is associated with many factors, such as the temperature of hydrothermal treatment, pH value and additives of the precursor solutions.

3.1. The hydrothermal temperature.

It has been reported that the morphologies of WO_3 nanomaterials by hydrothermal method are very sensitive to the preparation temperature[36-38]. In our study, the effects of hydrothermal temperature were also investigated. Figure 4 shows the FE-SEM images of products obtained under growth temperatures of 150°C, 180°C and 220°C. Distinguished with monodispersed nanobricks obtained at 200°C, it has been revealed that when the reaction temperature is relatively low or high (say, 150°C, 180°C or 220°C), the products are the mixtures of several nanostructures, which are two or more types of nanoparticles, cracked nanoplates, nanorods, and irregular nanobricks. Also, a rectangular nanobrick can be observed for products obtained at 180°C, denoted by an arrow in Figure 4b. A tendency is obviously shown that dimensions of primary nanostructures become larger as hydrothermal temperature increased, as clearly shown in Figure 4. And only when the hydrothermal reaction takes place at an

appropriate temperature (about 200°C) can we obtain the nearly mono-dispersed and pure WO_3 nanobricks (see Figure 3).

3.2 pH value of the precursor solution.

It has been found that the pH value of the colloidal precursor solution has an important effect on the morphologies of the products after the hydrothermal reaction. The freshly obtained colloidal solution (pH = 3.0) were acidified to the pH of 2.0 or lower, before hydrothermal treatments at 200 °C for 10 h. When pH = -0.6, the products are the mixture consisting of the dominant nanobricks and small amount of nanoparticles, nanoplates and nanowires, as typically seen in Figure 5a. Compared with those shown in Figure 3, dimensions of the nanobricks in the mixture products were only insignificantly decreased. When the pH was increased up to 2.0, the products were also well-dispersed particles. A close observation has illustrated that the products are mainly irregular naobricks with *ca.* 250 nm in size and surface-stepped structures, together with some much smaller nanoparticles, as exhibited in Figure 5b. By using the pristine LAL-induced colloidal solution without acidification (pH = 3.0), the products were dispersed nanoplates with polygonal morphology and 1-2μm in planar dimension (Figure 5c). There also exist the surface steps on the nanoplates. The further characterization for the fragmented nanosheets, which were scrapped from the nanoplates' planar surface, was performed through high resolution TEM, as shown in Figure 5d. The scrapped nanosheets exhibite the clear lattice fringes. The interplanar spacings of 0.368 and 0.388 nm correspond to the crystal planes (200) and (002) of orthorhombic $WO_3 \cdot 0.33H_2O$ phase (JCPDS No.

72-0199), respectively. The measured angle (90^o) between the [200] and [002] directions is well consistent with the crystallographic data. Correspondingly, XRD measurements have revealed that phase structure of the final products depends on the pH values, as illustrated in Figure 6. When the pH is 1.0 or smaller, the crystal phase of products is monoclinic WO_3, while for that of pH = 2.0 or higher the final products are the orthorhombic $WO_3 \bullet 0.33H_2O$ phase.

On basis of the above results, it can be concluded that with increasing the pH value of the precursor solution, the thickness of nanobricks decreases and evolve morphologically from nanobrick to nanoplate, keeping surface-stepped structure. Also, the higher pH conditions lead to hydrated tungsten oxide.

3.3. Additives in the precursor

For the fabrication of WO_3 nanomaterial via hydrothermal approach, diverse metal salts were usually added as capping agents to modulate crystal phases, architectures and dimensions of finally obtained products, as previously reported[13, 14, 39]. In our experiments, it has been found that addition of some amount of salts into the precursor solution lead to significant morphological changes and cannot induce formation of the nanobricks.

Figure 7 shows some typical results corresponding to the pristine precursor solutions (pH = 3.0, Figure 7a and 7b) and acidified ones (pH=1.0, Figure 7c and 7d) containing 0.6 mM NaCl or KCl as additives. All the products show hierarchical architectures and completely different from results without metal salts additives. Furthermore, the dimensions of hierarchical architectures by adding NaCl as additives

for both pristine and acidified precursors are obviously larger than that of KCl additives. These two additives probably act as capping or structure directing agents in hydrothermal processes.

4. Rectangular cuboidal stacking growth model

As mentioned above, the LAL-induced colloidal solution, which was composed of W-O isopolyanions and amorphous isopolytungstic acid nanoparticles with *ca.* 1 nm in size, was subsequently acidified and hydrothermally treated at 200°C. Under the acidic and hydrothermal conditions, the following reactions would take place:

$$H^{+}_{(low\ concen.)} + [W_{xy}O_{(m+n)y}]^{(2ny)-} + H_2O \rightleftharpoons W_xO_m \bullet nH_2O \qquad (6)$$

$$H^{+}_{(high\ concen.)} + [W_{xy}O_{(m+n)y}]^{(2ny)-} + W_xO_m \bullet nH_2O \rightleftharpoons WO_3 + H_2O \qquad (7)$$

The W-O isopolyanions would hydrate and polymerize to form the isopolytungstic acid [reaction (6)]. Further, for the higher [H^+] concentration (pH≤1.0 in our experiment), reaction (7) would occur under hydrothermal condition, or the formed isopolytungstic acid would dehydrate into tungsten oxide. In this case, the isopolytungstic acid ultra-fine nanoparticles would be gradually crystallized into WO_3 phase, which subsequently grow by consumption of the W-O isopolyanions in the solution according to reactions (6, 7)

4.1 Formation of the nanosized rectangular WO_3 cuboids.

According to the Bravais law, the crystal planes with high reticular density tend to be the exposed surfaces during crystal growth, i.e., the direction, along which interplanar spacing is larger, owns a lower growth rate. The is also consistent with the law that well-developed architectures usually own the minimized surface energy.[40]

For monoclinic WO_3 structure, the interplanar distances of different planes own an order of d (001) > d(010) > d(100). So, under an appropriate condition or quasi-equilibrium growth condition, the initial WO_3 phase would grow, by consumption of the W-O isopolyanions in the solution, preferentially along the directions [100], [010] and [001] in turn, forming the rectangular cuboid WO_3 with nanosized dimensions, as shown in Figs.8(a, b).

4.2 Stacking growth.

As the hydrothermal reaction is going, in addition to the normal growth by W-O isopolyanion-attachemnt, such nanosized rectangular cuboids would be stacked and linked together along the above three directions to minimize the surface energy, similar to the oriented connection growth[41-47] (Fig. 8c). Finally, the nanobricks with dimensions of several hundred nanometers and lower surface energy are formed (Fig. 8d and Fig.3). The stepped structure on the planar surface of the nanobricks should be the indications of the stacking growth. The possible grooves, from the link or oriented connection between the initial nanosized rectangular cuboids would disappear after enough long time, due to the preferential attachment of the WO_3 molecules on them, which originate from the W-O isopolyanion (reaction 7).

As for the influence of some factors, under lower [H^+] concentration conditions (pH = 2.0 and 3.0), only reaction (6) would take place and hence the hydrated tungsten oxide $WO_3 \cdot 0.33H_2O$ was obtained. Under the lower (150^{o}C, 180^{o}C) or higher (220^{o}C) reaction temperature, too slow or too fast growth could take place, inducing the mixture of the nanobricks and some nanosized particles which have not

yet stacked together (see Fig.4). Under addition of metal salts, the cations or anions in the precursor would act as capping or structure directing agents, leading to completely different morphologies.

CONCLUSION

In summary, the rectangular brick-like nanostructured tungsten oxide (WO_3) has been fabricated based on laser ablation of tungsten flake in water and subsequent hydrothermal route. The nanobricks are, in the average dimensions, of *ca.* 200 nm in length, 150 nm in width and 130 nm in thickness. It has found that the reaction temperature, pH value and composition of the precursor in subsequent hydrothermal treatment are important to formation of the brick-like WO_3 nanostructures. Only the appropriate temperature (~200^{o}C) and pH value (~1.0) lead to the nanobricks. Formation of the nanobrick can be described by a rectangular cuboidal stacking growth model or the nanosized rectangular WO_3 cuboids' formation and subsequent stacking growth. The combination of laser ablation in liquid with hydrothermal treatment could provide an effective way to fabricate the morphologically tunable WO_3 nanomaterials. The WO_3 nanobricks might be the good building blocks of complex micro/nanostructures and devices, such as electrochromic electrodes, chemical sensors and so on.

ACKNOWLEDGMENT

This work is financially supported by the National Basic Research Program of China

(Grant No.2012CB932303), Recruitment Program of Global Experts (C), the Natural Science Foundation of China (Grant No. 51371165, 11374303), China Postdoctoral Science Foundation (Grant No. 2013M540525) and Anhui Provincial Natural Science Foundation for Distinguished Young Scholar (Grant No. 1108085J20).

REFERENCES

1. J. Kukkola, J. Maklin, N. Halonen, T. Kyllonen, G. Toth, M. Szabo, A. Shchukarev, J. P. Mikkola, H. Jantunen and K. Kordas, *Sens. Actuator B-Chem.*, 2011, **153**, 293-300.

2. X. Q. Gao, X. H. Rao, J. D. Wang, F. Xiao and X. T. Su, *Prog. Chem.*, 2013, **25**, 105-114.

3. G. Gu, B. Zheng, W. Q. Han, S. Roth and J. Liu, *Nano Lett.* , 2002, **2**, 849-851.

4. H. W. Zhang, G. T. Duan, G. Q. Liu, Y. Li, X. X. Xu, Z. F. Dai, J. J. Wang and W. P. Cai, *Nanoscale*, 2013, **5**, 2460-2468.

5. S. H. Baeck, K. S. Choi, T. F. Jaramillo, G. D. Stucky and E. W. McFarland, *Adv. Mater.* , 2003, **15**, 1269-1273.

6. G. A. Niklasson and C. G. Granqvist, *J. Mater. Chem.* , 2007, **17**, 127-156.

7. J. Polleux, A. Gurlo, N. Barsan, U. Weimar, M. Antonietti and M. Niederberger, *Angew. Chem.-Int. Edit.*, 2006, **45**, 261-265.

8. Z. F. Liu, M. Miyauchi, T. Yamazaki and Y. B. Shen, *Sens. Actuator B-Chem.*, 2009, **140**, 514-519.

9. J. H. Lee, J. Kim, H. W. Seo, J. W. Song, E. S. Lee, M. Won and C. S. Han, *Sens. Actuator B-Chem.*, 2008, **129**, 628-631.

10. Z. Xie, Y. G. Zhu, J. Xu, H. T. Huang, D. Chen and G. Z. Shen, *Crystengcomm*, 2011, **13**, 6393-6398.

11. H. Kominami, K. Yabutani, T. Yamamoto, Y. Kara and B. Ohtani, *J. Mater. Chem.* , 2001, **11**, 3222-3227.

12. Z. G. Zhao and M. Miyauchi, *Angew. Chem.-Int. Edit.*, 2008, **47**, 7051-7055.

13. J. Zhang, J. P. Tu, X. H. Xia, X. L. Wang and C. D. Gu, *J. Mater. Chem.* , 2011, **21**, 5492-5498.

14. X. C. Song, Y. F. Zheng, E. Yang and Y. Wang, *Mater. Lett.* , 2007, **61**, 3904-3908.

15. A. Z. Sadek, H. D. Zheng, M. Breedon, V. Bansal, S. K. Bhargava, K. Latham, J. M. Zhu, L. S. Yu, Z. Hu, P. G. Spizzirri, W. Wlodarski and K. Kalantar-zadeh, *Langmuir*, 2009, **25**, 9545-9551.

16. H. W. Zhang, G. T. Duan, Y. Li, X. X. Xu, Z. F. Dai and W. P. Cai, *Cryst. Growth Des.*, 2012, **12**, 2646-2652.

17. M. Shibuya and M. Miyauchi, *Chem. Phys. Lett.* , 2009, **473**, 126-130.

18. Y. L. Ma, L. Zhang, X. F. Cao, X. T. Chen and Z. L. Xue, *Crystengcomm*, 2010, **12**, 1153-1158.

19. A. Yella, U. K. Gautam, E. Mugnaioli, M. Panthoefer, Y. Bando, D. Golberg, U. Kolb and W. Tremel, *Crystengcomm*, 2011, **13**, 4074-4081.

20. F. Zheng, M. Guo and M. Zhang, *Crystengcomm*, 2013, **15**, 277-284.

21. H. G. Choi, Y. H. Jung and D. K. Kim, *J. Am. Ceram. Soc.* , 2005, **88**, 1684-1686.

22. H. A. Therese, J. X. Li, U. Kolb and W. Tremel, *Solid State Sci.* , 2005, **7**, 67-72.

23. D. L. Chen, L. Gao, A. Yasumori, K. Kuroda and Y. Sugahara, *Small*, 2008, **4**, 1813-1822.

24. H. Wang, X. Quan, Y. B. Zhang and S. Chen, *Nanotechnology*, 2008, **19**, 065704-065709.

25. Z. J. Gu, T. Y. Zhai, B. F. Gao, X. H. Sheng, Y. B. Wang, H. B. Fu, Y. Ma and J. N. Yao, *J. Phys. Chem. B* 2006, **110**, 23829-23836.

26. D. Chen and J. H. Ye, *Adv. Funct. Mater.* , 2008, **18**, 1922-1928.

27. Y. Zhang, Y. G. Chen, H. Liu, Y. Q. Zhou, R. Y. Li, M. Cai and X. L. Sun, *J. Phys. Chem. C* 2009, **113**, 1746-1750.

28. W. T. Wu, J. S. Chen and J. J. Wu, *J. Am. Ceram. Soc.* , 2010, **93**, 2268-2273.

29. S. K. Yang, W. P. Cai, H. W. Zhang, X. X. Xu and H. B. Zeng, *J. Phys. Chem. C* 2009, **113**, 19091-19095.

30. P. S. Liu, W. P. Cai and H. B. Zeng, *J. Phys. Chem. C* 2008, **112**, 3261-3266.

31. U. K. Gautam, S. R. C. Vivekchand, A. Govindaraj, G. U. Kulkarni, N. R. Selvi and C. N. R. Rao, *J. Am. Chem. Soc.* , 2005, **127**, 3658-3659.

32. G. W. Yang, *Prog. Mater Sci.* , 2007, **52**, 648-698.

33. H. B. Zeng, X. W. Du, S. C. Singh, S. A. Kulinich, S. K. Yang, J. P. He and W. P. Cai, *Adv. Funct. Mater.* , 2012, **22**, 1333-1353.

34. C. T. Szymanski, *Mineral*, 1984, **22**, 681-688.

35. A. Chemseddine and U. Bloeck, *J. Solid State Chem.* , 2008, **181**, 2731-2736.

36. J. Pfeifer, G. F. Cao, P. Tekulabuxbaum, B. A. Kiss, M. Farkasjahnke and K. Vadasdi, *J. Solid State Chem.* , 1995, **119**, 90-97.

37. B. Gerand, G. Nowogrocki and M. Figlarz, *J. Solid State Chem.* , 1981, **38**, 312-320.

38. C. Balazsi and J. Pfeifer, *Solid State Ion.*, 2002, **151**, 353-358.

39. J. M. Wang, P. S. Lee and J. Ma, *Cryst. Growth Des.*, 2009, **9**, 2293-2299.

40. X. H. Huang, Z. Y. Zhan, X. Wang, Z. Zhang, G. Z. Xing, D. L. Guo, D. P. Leusink, L. X. Zheng and T. Wu, *Appl. Phys. Lett.* , 2010, **97**, 2031121-2031123.

41. B. A. Korgel and D. Fitzmaurice, *Adv. Mater.* , 1998, **10**, 661-665.

42. Z. Y. Tang, N. A. Kotov and M. Giersig, *Science*, 2002, **297**, 237-240.

43. K. S. Cho, D. V. Talapin, W. Gaschler and C. B. Murray, *J. Am. Chem. Soc.* , 2005, **127**, 7140-7147.

44. N. Pradhan, H. F. Xu and X. G. Peng, *Nano Lett.* , 2006, **6**, 720-724.

45. M. Ethayaraja and R. Bandyopadhyaya, *Langmuir*, 2007, **23**, 6418-6423.

46. H. B. Zeng, P. S. Liu, W. P. Cai, X. L. Cao and S. K. Yang, *Cryst. Growth Des.*, 2007, **7**, 1092-1097.

47. X. Y. Chen, Y. Zhou, Q. Liu, Z. D. Li, J. G. Liu and Z. G. Zou, *ACS Appl. Mater. Interfaces* 2012, **4**, 3372-3377.

Tungsten Oxide Nanostructures Based on Laser Ablation in Water and Hydrothermal Route

Hongwen Zhang, Yue Li [*], Guotao Duan, Guangqiang Liu and Weiping Cai [*]

Key Lab of Materials Physics, Anhui Key Lab of Nanomaterials and Nanotechnology, Institute of Solid State Physics, Chinese Academy of Sciences, Hefei 230031, P.R. China.

Figures and Captions

Figure 1 Characterization of the LAL-induced colloidal solution. (a) Optical absorbance spectrum. (b) TEM observations. The insets are a highly magnified TEM image and the corresponding SAED pattern. (c) Corresponding EDX spectrum.

Figure 2 XRD patterns of the final products (pH = 1.0, 200 ^{o}C, 10 h) and the standard pattern of the monoclinic WO_3 powders (line spectrum).

Figure 3 Morphology and microstructure of the final products (pH = 1.0, 200 ^{o}C, 10 h). (a, b): FE-SEM images. The inset in (b) is a local magnified image. (c): TEM and (d): high resolution TEM images. Insets in (c) are the SAED pattern (up-left) acquired from the direction as the arrow indicates, and an isolated nanobrick (down-right).

Figure 4 FE-SEM images of the products after hydrothermal treatment of LAL-induced precursors (pH = 1.0) at (a) 150 ^{o}C , (b) 180 ^{o}C and (c) 220 ^{o}C for 10 hours.

Figure 5 The morphological dependence on pH value of the precursor soloution. The FE-SEM observations of the products corresponding to the precursor soloutions with

pH values -0.6 (a), 2.0 (b), and 3.0 (c), respectively. The insets in (c) are isolated nanoplates with higher magnification. (d): TEM observations of the isolated nanosheets that flake off surface of nanoplates in (c).

Figure 6 XRD patterns of the products after hydrothermal treatment of the precursor solutions with pH = -0.6 (a) and 2.0 (b). (c): standard pattern of orthorhombic $WO_3 \cdot 0.33H_2O$.

Figure 7 FE-SEM images of the products after hydrothermal treatment of the 30 ml pristine and acidified colloidal solutions containing 0.6mM NaCl or KCl as additives. (a) pH=3.0, NaCl; (b) pH=3.0, KCl; (c) pH=1.0, NaCl; (d) pH=1.0, KCl. The insets in (a) and (c): corresponding local magnified images.

Figure 8 Schematic illustration for the rectangular cuboidal stacking growth model. (a): crystallization of isopolytungstic acid ultra-fine nanoparticles into WO_3, or formation of WO_3 crystal nuclei. (b): the nanosized rectangular cuboids. (c): Stacking of the nanosized rectangular cuboids. (d): Formation of surface-stepped nanobrick. Step I: Growth of WO_3 nuclei preferentially along [100], [010] and [001] directions in turn. Steps II and III: Continuous stacking of the nanosized rectangular cuboids.

Figure 1 Zhang H. W. et al

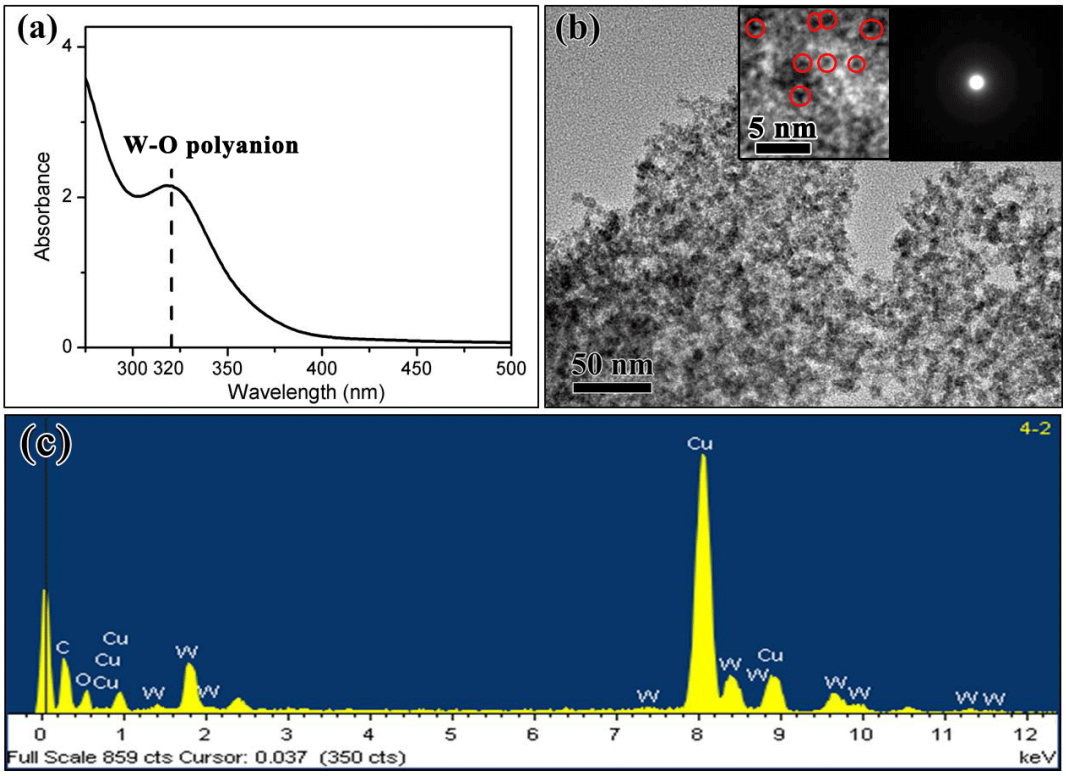

Figure 2 Zhang H. W. et al

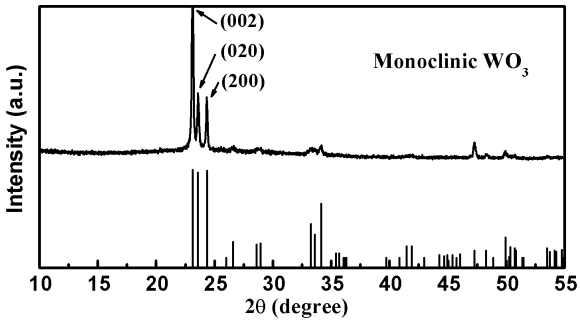

Figure 3 Zhang H. W. et al

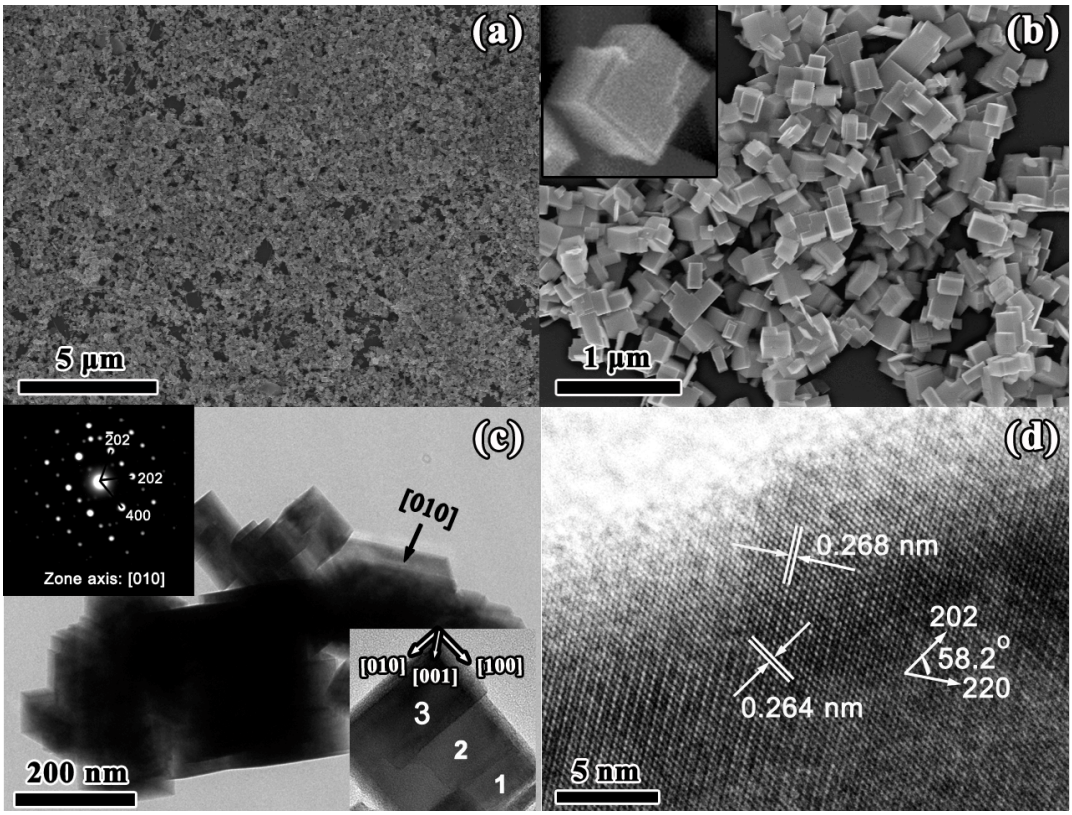

Figure 4 Zhang H. W. et al

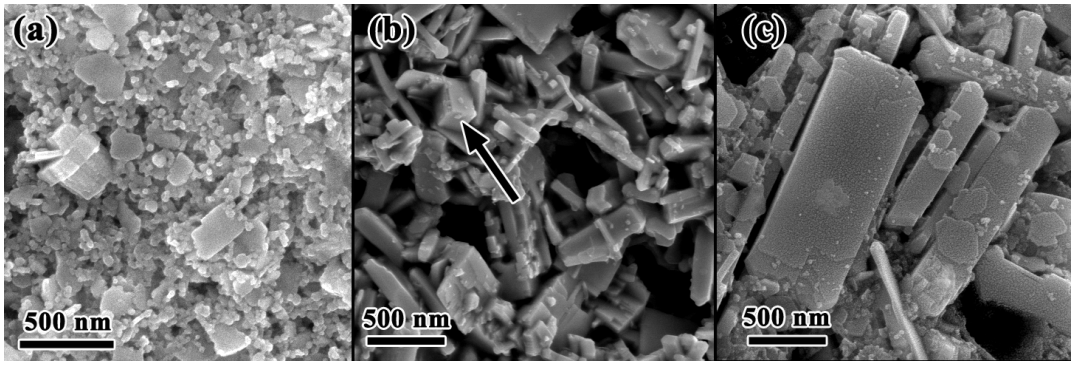

Figure 5 Zhang H. W. et al

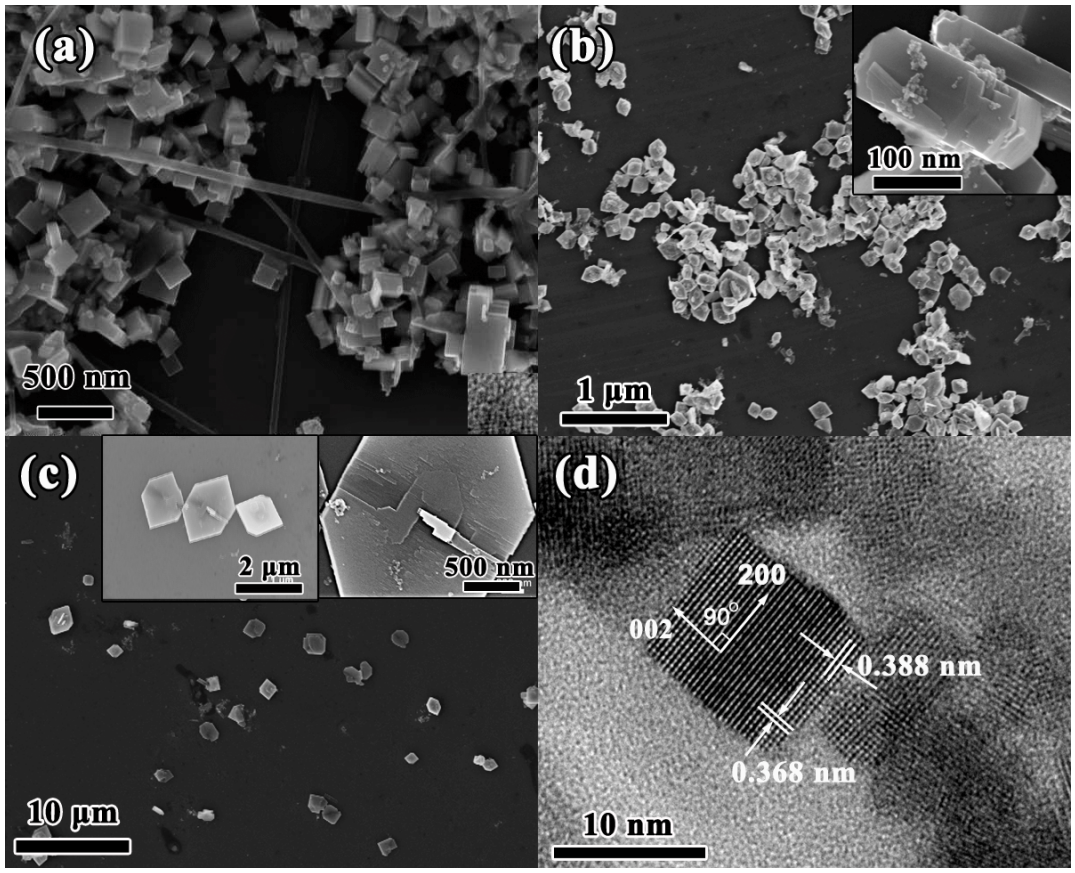

Figure 6 Zhang H. W. et al

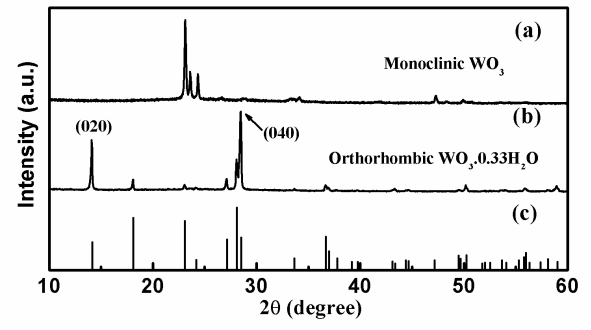

Figure 7 Zhang H. W. et al

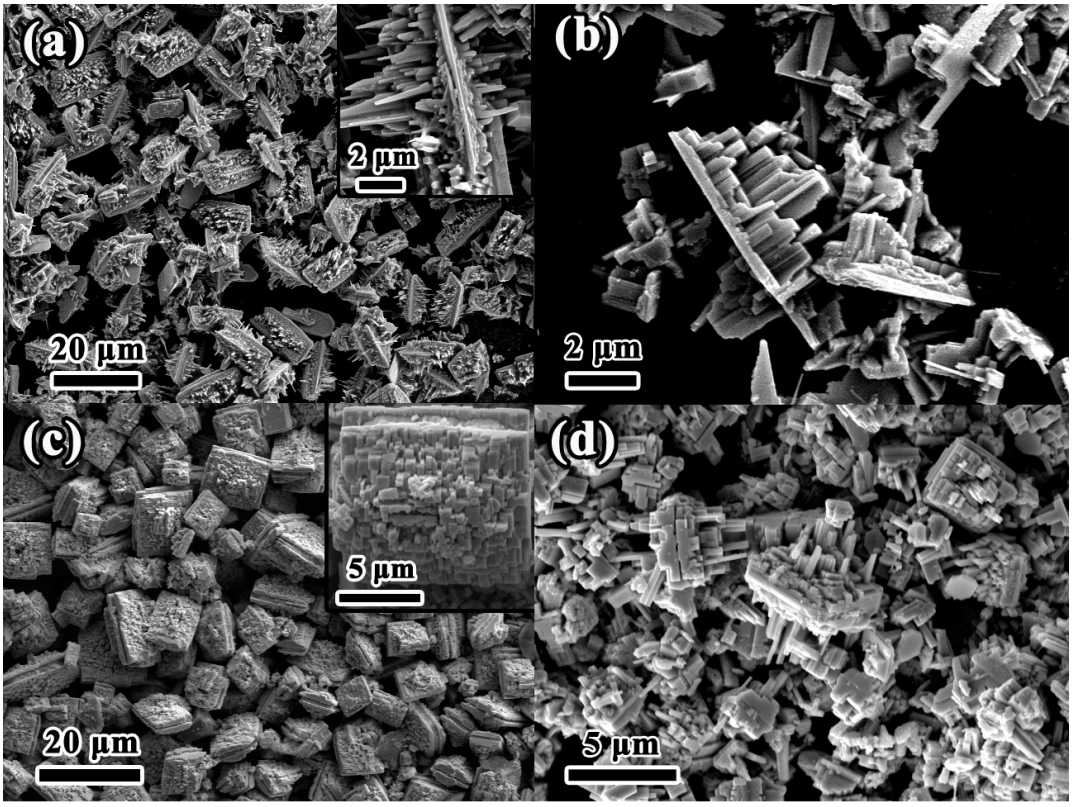

Figure 8 Zhang H. W. et al